International Journal of Scientific Research in Chemical Sciences
Vol.**12**, Issue.**3**, pp.**08-15**, June **2025**
E-ISSN: 2455-3174
Available online at: www.isroset.org

Research Article

QSAR, Molecular Docking Study, Drug- Likeness and ADMET of Tanshinone Derivatives as Anti- prostate Cancer Compounds

Abdulrahman Ibrahim Kubo[1*], Saminu M. A[2]

[1]Department of Chemistry, Faculty of Sciences, Adamawa State University, Mubi, Nigeria
[2]Department of Chemistry, Faculty of Sciences, Adamawa State University, Mubi, Nigeria

**Corresponding Author:* ✉ *abdulrahmankuboibrahim@gmail.com*

Received: 13/Jun/2025; **Accepted**: 25/Jun/2025; **Published**: 30/Jun/2025. | **DOI**: https://doi.org/10.26438/ijsrcs.v12i3.194

Abstract— Cancer remains one of the leading causes of death worldwide, with the global cancer mortality rate continuing to rise. Projections estimate approximately 12 million deaths by 2030. Prostate cancer, in particular, stands out as a major contributor to cancer-related mortality, with its incidence steadily increasing over the past decade. This study aims to construct a quantitative structure- activity relationship (QSAR) model for the development of a highly effective and robust anti-prostate cancer agent targeting the LNCaP cell line. Model One was found to be predictive, powerful, and reliable, based on the following statistical parameters: coefficient of determination (R^2) = 0.9916, adjusted R^2 = 0.9878, standard error of estimation (SEE) = 0.346, mean absolute error (MAE) = 0.035, and concordance correlation coefficient (CCC) = 0.9238. Additionally, the model demonstrated anticancer activity of tanshinone derivatives based on the THSA, MLFER_E, ASP-3, AVP-7, and TDB1v descriptors. Molecular docking results revealed that the docking scores of the three most promising compounds ranged from (-10.4 to -10.6) kcal/mol. These findings suggest that the selected compounds hold significant potential for predicting the anti-proliferative effects of other tanshinone derivatives against the LNCaP prostate cancer cell line.

Keywords— QSAR, ADMET, LNCap, Prostate cancer, Docking, Drug- likeness

1. Introduction

Cancer continues to be a leading cause of mortality worldwide. The global cancer mortality rate is steadily rising, with projections estimating approximately 12 million deaths by 2030 [1]. Cancer cells differ significantly from their normal counterparts in various biochemical processes, particularly in cell division and growth regulation. A key characteristic of most cancer cells is their high rate of proliferation. Therefore, targeting pathways involved in uncontrolled cell division which ultimately trigger apoptosis has emerged as a promising avenue in cancer therapy [2]. The ideal anti-cancer drugs should selectively destroy cancer cells without causing significant harm to healthy tissues [3].

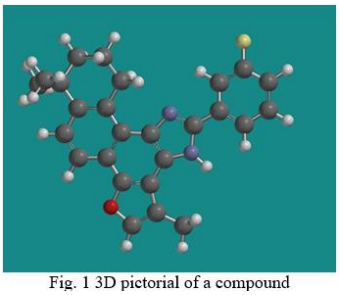

Fig. 1 3D pictorial of a compound

However, these treatments can also damage certain normal, proliferating cell, which has motivated the global search for safer and more effective therapeutic options for cancer prevention and treatment. Prostate cancer ranks among the most common malignancies in men globally and is a significant contributor to cancer-related deaths. Its incidence has steadily increased over the past decade [4]. This form of cancer originates in the prostate gland and predominantly affects older males. According to GLOBOCAN (2018), prostate cancer is the second most diagnosed cancer in men, with 1,276,106 new cases and 358,989 deaths reported worldwide, with higher rates observed in developed nations. By 2030, due to global population growth, the number of new cases is expected to rise to 1.7 million, with deaths projected to reach 499,000 [5], [6], [7].

Despite the use of various anti-cancer drugs either alone or in combination with radiotherapy no conventional treatment has proven highly effective against advanced prostate cancer [8]. Studying the progression of prostate cancer from its early to advanced stages remains a significant challenge in vitro. A seminal study by Horoszewicz and colleagues introduced the

LNCaP prostate cancer cell line, which continues to be one of the few, if not the only, human cell lines capable of simulating a broad spectrum of prostate cancer stages. This includes the transition from androgen sensitivity to castration-resistant states, metastasis to bone, and varying responses to drug treatments [9]. The most widely used human prostate cancer cell lines are PC3, DU145, and LNCaP [10]. Among these, only LNCaP cells express the androgen receptor and respond to androgens. This androgen responsiveness is a key reason why LNCaP cells are uniquely suited for modeling the progression of prostate cancer.

Over the years, many drugs have been discovered through random screening and the serendipitous identification of natural compounds effects on various diseases. Although this traditional approach has limitations, it has significantly contributed to the development of many essential drugs. However, the drug discovery process is typically lengthy, resource-intensive, and costly, involving several stages from target identification to final drug approval [11]. To improve the efficiency of drug development, researchers are increasingly relying on modern technologies and innovative methodologies [12]. The development of new anti-prostate cancer agents has become particularly critical given the diseases rising prevalence [13], [14] and the rapid emergence of multidrug resistance, which significantly hampers the effectiveness of current chemotherapies [15], [16]. Tanshinones, specifically Tanshinone I (Tan I) and Tanshinone IIA (Tan IIA), have shown potent anti-cancer activity against various malignancies, including cancers of the bladder [17], cervix [18], liver [19], [20] pancreas, and prostate [21], [22], [23], [24], [25]. Additionally, derivatives of these compounds have demonstrated effectiveness in limiting the invasiveness and metastatic potential of prostate cancer cells [26].

In silico approaches have proven useful in elucidating the molecular mechanisms of interactions between small molecules and target proteins. Accordingly, molecular docking and pharmacokinetic analyses including assessments of drug-likeness based on Lipinski's Rule of Five and ADMET profiling were performed on selected Tanshinone derivatives. These studies aimed to evaluate their potential against castration-resistant prostate cancer using the LNCaP cell line and targeting the 5T8E protein receptor, with the goal of describing their binding affinities and interaction profiles.

2. Method

2.1. Data collection

The 23 tanshinone derivatives synthesized by Xu *et al.* [27] were assessed for their anticancer potential against the LNCaP prostate cancer cell line, and their inhibitory concentrations (IC_{50}) were transformed into logarithmic scale values (pIC_{50}) using Equation 1**.** These transformed inhibitory values were used in a comprehensive Quantitative Structure-Activity Relationship (QSAR) analysis to identify the most promising compounds with potent anti-prostate cancer activity.

$$pIC_{50} = -\log 10\ (IC_{50} \times 10^{-6}) \quad (1)$$

2.2. 2D Structure and geometry optimization

The molecular structures of the compounds were initially sketched using ChemDraw v12.0 and subsequently imported for Density Functional Theory (DFT) calculations [28]. Geometry optimization was carried out using the B3LYP functional in combination with the 6-31G basis set in Spartan V14.1 [29].

2.3. Model generation

To construct the predictive models, Multiple Linear Regression (MLR) was applied to the training dataset in conjunction with the Genetic Function Approximation (GFA) technique. In this modelling approach, the biological activity values (pIC_{50}) served as dependent variables, while various calculated molecular descriptors were used as independent variables.

2.4. Model validation

In QSAR modeling, the most commonly used evaluation metrics include R^2 and R^2_{adj}. Although high values of these metrics are important, they alone are not sufficient to confirm model reliability [30]. To assess potential multicollinearity among the descriptors, the Variance Inflation Factor (VIF) was employed. A VIF value close to 1 indicates no correlation, values between 1 and 5 suggest an acceptable level of correlation, while values exceeding 10 indicate strong multicollinearity, rendering the model unacceptable. The VIF is defined as:

$$VIF = \frac{1}{(1-R^2)} \quad (2)$$

R^2 is the correlation coefficient of the selected descriptor [31]. All descriptors and their contributions to the model can be evaluated using their mean effect, which reflects the influence of individual descriptors in the developed equation. The signs of the model parameters indicate whether each descriptor contributes positively or negatively to the overall model outcome [32].

$$Mean\ Effect = \frac{\beta j \Sigma_i^n Dj}{\Sigma^{m(\beta j \Sigma_i^n Dj)}} \quad (3)$$

To assess the external validity of the developed model, a test set was used, and the Concordance Correlation Coefficient (CCC) was calculated, a CCC value greater than 0.8 is generally considered indicative of a reliable and predictive model. The CCC is defined as:

$$CCC = \frac{2\ \sum_{i=1}^{nEXT}(Yi - \bar{Y})\ (Yi - \bar{Y}i)}{\Sigma_{i=1}^{nEXT}(Yi - \bar{Y})^2 + \Sigma_{i=1}^{nEXT}(Yi - \bar{Y}i)^2 + nEXT\ (Yi - \bar{Y}i)^2}$$

$$CCC = \frac{2\ \sum_{i=1}^{nEXT}(Yi - \bar{Y})\ (Yi - \bar{Y}i)}{\Sigma_{i=1}^{nEXT}(Yi - \bar{Y})^2 + \Sigma_{i=1}^{nEXT}(Yi - \bar{Y}i)^2 + nEXT\ (Yi - \bar{Y}i)^2} \quad (4)$$

Where Y_i represents the experimental activity value, $\bar{Y}$ denotes the mean of the experimental values, $\hat{Y}_i$ is the predicted activity value, and $\bar{\hat{Y}}$ is the mean of the predicted

values. EXT refers to the external (test) set used for validation [33].

2.5. Y- randomization

Another key validation technique used to assess model robustness is the Y-randomization test**.** In this method, the dependent variables are randomly shuffled while the independent variables remain unchanged. The test is applied to the training set, and a valid model should yield significantly lower R^2 and Q^2 values compared to the original model. Such results confirm that the model is robust, reliable, and not the result of chance correlations.

2.6. Docking study

Molecular docking studies provided valuable insights into the interactions between ligands and the receptor, enabling the identification of the best-binding compounds based on their binding affinities. This approach was used to screen for the most promising candidates that demonstrated strong binding potential with the androgen receptor.

2.7. SwissADME (ADMET/Drug- likeness)

The top three compounds identified as the most active against the LNCaP cell line were further evaluated for their drug-likeness and ADMET properties using SwissADME and ADMET lab 2.0**.** Conducting such profiling in the early stages of drug discovery is essential for evaluating the therapeutic viability and development potential of candidate molecules.

3. Results and Discussion

This study analyzed a dataset comprising 23 tanshinone derivatives along with their biological activities to evaluate their potential as anti-prostate cancer agents. The dataset was divided using the Kennard-Stone algorithm, allocating 17 compounds to the training set and the remaining 6 compounds to the test set to evaluate the predictive performance of the developed models. A total of five QSAR models were generated through the integration of the Genetic Function Approximation (GFA) with Multiple Linear Regression (MLR)**.** Among these, Model 1 demonstrated the highest statistical robustness and was identified as the most reliable. To select the best QSAR equation, outputs from both the GFA and MLR methods were compared, with Model 1 providing the best overall results.

Model 1

pIC_{50} = 26.6675 (***THSA**) + 0.0012 (***MLFER_E**) - 2.4866 (***ASP-3**) - 131.6947 (***AVP-7**) - 1200.1564 (***TDB1v**) + 0.0372.

(R^2) = 0.9916, (R^2_{adj}) = 0.9878, (SEE) = 0.346, (MEA) = 0.035, (Q^2-LOO) = 0.9824 and (CCC) test = 0.9238

Model 1 was selected from the five developed models due to its superior statistical performance. It was employed to predict the anti-proliferative activities of the test set compounds, with the results detailed in Table 1**.** This model demonstrated excellent internal validation metrics based on the training set, including a high coefficient of determination (R^2) of 0.9916, adjusted R^2 of 0.9878, standard error of estimation (SEE) of 0.346, mean absolute error (MAE) of 0.0351, and a leave-one-out cross-validation coefficient (Q^2_LOO) of 0.9824. For external validation using the test set, the concordance correlation coefficient (CCC) was 0.9238, further supporting the model's robustness. Table 1 presents the binding energies, residuals, experimental pIC_{50} values**,** and predicted pIC_{50} values for all 23 tanshinone derivatives, calculated using Equation 1.

Table 2 displays the definitions of the descriptors included in the final QSAR model. The model contains 2D topological descriptors MLFER_E**,** ASP-3, and AVP-7 which are defined as excessive molar refraction**,** average simple path order 3, and average valence path order 7**,** respectively, and describe the molecular structure based on atomic connectivity. The model also includes 3D geometrical descriptors**:** THSA**,** defined as the sum of the solvent-accessible surface area of atoms with absolute partial charges less than 0.2. It characterizes a molecule in terms of the atom types present and the spatial coordinates of each atom. TDB1v**,** defined as the 3D topological distance-based autocorrelation lag 1 weighted by Van der Waals volume**,** reflects hydrogen bonding potential and its importance in relation to atom pairs separated by one bond (lag 1), which influences tanshinone activity against the LNCaP prostate cancer cell line.

The mean effect (ME) obtained from the model parameters indicates that THSA **a**nd TDB1v have positive coefficients, suggesting that increasing these descriptors enhances the biological activity of the compounds. In contrast, MLFER_E**,** ASP-3**,** and AVP-7 have negative coefficients**,** implying that reducing these values would similarly enhance the activity of the tanshinone derivatives against the LNCaP cell line. Table 3 presents the results of the Y-randomization test, which shows low values of R^2 and Q^2, confirming that the model's robustness is not due to random chance. Table 4 provides statistical analyses, highlighting the correlation between individual descriptors and their contributions to the model. The scatter plot of standardized residuals versus experimental activity, presented in Figure 2**,** shows a symmetrical distribution of data points on both sides of zero. This indicates a lack of systematic bias and confirms the model's reliability. Additionally, the scatter plot comparing observed and predicted biological activities, shown in Figure 3**,** demonstrates that the data points closely follow the trend line, indicating strong predictive accuracy.

3.1 Docking results

Docking simulations were performed between 23 tanshinone compounds and the active binding site of the androgen receptor (PDB ID: 5T8E). AutoDock via PyRx software was used to predict interactions between target macromolecules and candidate ligands, facilitating the identification of potential ligand–receptor combinations. The tanshinone derivatives underwent docking studies to assess their binding affinities with the androgen receptor (5T8E). As a result, three lead compounds with the most favorable binding scores

were identified. These compounds exhibiting docking scores ranging from (-10.4 to -10.6 kcal/mol) are displayed in Table 5, which also presents their binding affinities, bond distances, and the specific amino acid residues involved in the interactions. These values indicate strong interactions between the top inhibitors and the androgen receptor, primarily involving hydrogen bonding, hydrophobic interactions, and electrostatic interactions. The 2D and 3D visual representations and spatial analyses of these ligand–receptor interactions within the androgen receptor binding site were generated using Discovery Studio software. These top three active compounds were selected for further analysis.

Compound 19 exhibited the most favorable binding energy of (-10.6 kcal/mol). It formed one conventional hydrogen bond with GLU683 (4.72 Å), a Pi-donor electrostatic interaction with ASN756 (6.48 Å), and a Pi-cation interaction with ARG752 (4.72 Å). Additional hydrophobic interactions included a Pi- Pi T-shaped interaction with TRP751 (6.70 Å) and several Pi- alkyl interactions with TRP751 (6.03 Å), VAL684 (6.43 Å), ARG752 (4.85, 5.42, and 6.03 Å), ALA748 (4.24 Å), and PRO628 (4.45 Å). The 2D and 3D representations of Compound 19 bound to the 5T8E receptor, shown in Figure 4, illustrate these interactions and highlight the compound's strong binding affinity.

Compound 5, with the second-best docking score of (-10.5 kcal/mol), also demonstrated a robust interaction profile. It formed a conventional hydrogen bond with GLU681 (4.61 Å) and a Pi-cation electrostatic interaction with ARG752 (5.34 Å). Hydrophobic interactions included alkyl contacts with LEU815 (6.38 Å), VAL715 (4.55 Å), TRP751 (5.95 Å), and ALA748 (5.23 Å), as well as Pi-alkyl interactions with PRO682 (4.41 Å) and ARG752 (6.05, 5.51, and 4.93 Å). These docking conformations and interactions are depicted in Figure 5.

Compound 8, with a docking score of (-10.4 kcal/mol), also exhibited strong binding characteristics with the androgen receptor. It formed a hydrogen bond with GLU681 (4.64 Å), a Pi-cation interaction with ARG752 (5.30 Å), and a Pi-donor interaction with ASN756 (6.40 Å). Hydrophobic contacts included a Pi- Pi T-shaped interaction with TRP751 (6.49 Å) and alkyl interactions with VAL715 (5.08 Å), ALA748 (5.27 Å), LEU805 (6.42 Å), and TRP751 (6.03 Å). Additionally, Pi-alkyl interactions were observed with PRO682 (4.45 and 4.51 Å) and ARG752 (4.93, 5.50, and 5.97 Å). The corresponding 2D and 3D docking visuals are presented in Figure 6.

Interestingly, a closer examination of the 2D interaction diagrams (Figures 4- 6) reveals that several amino acid residues which do not directly bind to the ligands may still influence ligand-receptor interactions **i**ndirectly. These residues may interact with amino acids that are directly involved in binding, thereby contributing to the overall stabilization and binding affinity of the ligand- receptor complex.

3.2 SwissADME/ ADMET Results

A summary of the calculated ADME-related molecular descriptors for the top compounds, focusing on drug-likeness and ADMET behavior, is presented in Tables 6 and 7. All three compounds particularly compounds 5 and 8 exhibited a low number of hydrogen bond donors and acceptors. These favorable values support the overall pharmacokinetic profiles of the molecules, aligning well with desirable drug-likeness characteristics. A high number of hydrogen bond donors and acceptors generally reduce membrane permeability, as greater desolvation energy is required for the molecules to transition from aqueous environments into lipid membranes [34].

The blood- brain barrier (BBB) serves as a crucial defense mechanism for the central nervous system (CNS), maintaining homeostasis by controlling the exchange between systemic blood and the brain. For drugs that are not intended to target the CNS, such as those studied here, a low BBB penetration value is preferred, as it reduces the likelihood of CNS-related side effects [35], [36]. As shown in Table 7, compounds 19, 5, and 8 all demonstrated low BBB penetration values. According to the literature [37], a BBB value below 1 (brain/blood < 1) indicates poor CNS penetration, classifying the compound as CNS-inactive an appropriate property for drugs not targeting the brain. Additionally, the Caco-2 cell model was employed to estimate the oral absorption potential of the compounds in humans. This model mimics passive drug diffusion across intestinal epithelial cells and is widely adopted for assessing drug permeability and absorption [38], [39].

Table 1: Binding energy, experimental pIC50, predicted pIC50 data for 23 Tashinone derivatives

S/No	Experimental pIC_{50}	Predicted pIC_{50}	Residues	Binding energy (kcal/mol)
*1	5.1487	6	0.8513	-10.2
2	5.0861	5.6989	0.6128	-10.2
3	5.2006	5.5228	0.3222	-10.2
4	5.0409	5.3979	0.357	-10.2
5	5.0969	5.3012	0.2043	-10.5
6	5.1426	5.2218	0.0792	-10.2
7	5.0915	5.1549	0.0634	-10.2
*8	5.0222	5.0969	0.0749	-10.4
9	5.2291	5.0457	-0.1834	-10.1
10	5.1249	5	-0.1249	-9.9
11	5.0757	4.9586	-0.1171	-9.8
12	5.2365	4.9208	-0.3157	-9.4
13	5.1938	4.8860	-0.3078	-7.6
*14	5.6575	4.8538	-0.8037	-9.9
15	5.7447	4.8239	-0.9208	-10.2
16	5.8239	4.7958	-1.0281	-10.1
*17	5.4685	4.7695	-0.699	-10.2
18	5.2757	4.7447	-0.531	-9.8
*19	5.3767	4.7212	-0.6555	-10.6
20	5.8538	4.6989	-1.1549	-8.1
*21	5.7958	4.6777	-1.1181	-10.1
22	6.3872	4.6575	-1.7297	-7.3
23	6.1674	4.6382	-1.4842	-10.2

*Denote test set

Table 2: Descriptors, definition and class for the build model 1

Descriptors	Definition	Class
THSA	Sum of solvent accessible surface area	3D

	of atoms with absolute value of partial charges less than 0.2	
MLFER_E	Excessive molar refraction	2D
ASP-3	Average simple path, order 3	2D
AVP-7	Average valence path, order 7	2D
TDB1v	3D topological distance based autocorrelation- lag 1/ weight by van der waals volume	3D

Table 3: Y- randomization

Model type	R^2	Q^2-LOO
Original	0.991631	0.98236
Random 1	0.116903	-1.45933
Random 2	0.405836	-0.26787
Random 3	0.325475	-0.51945
Random 4	0.377133	-0.87319
Random 5	0.342468	-0.8214
Random 6	0.322453	-0.70271
Random 7	0.241257	-1.05561
Random 8	0.348599	-0.57256
Random 9	0.3774	-0.5928
Random 10	0.305077	-0.69085
Summary:		
R^2	Original Model	0.991631
Q^2-LOO	Original Model	0.98236
Average R^2	10 Random Models	0.31626
Average Q^2-LOO	10 Random Models	-0.75558

Table 4: Statistical analysis of model 1 parameters

	THSA	*MLFER_E*	*ASP-3*	*AVP-7*	*TDB1v*	*VIF*	*M/E*
THSA	1	0.006	0.075	-0.130	-0.348	1.354	-0.054
MLFER_E	0.006	1	-0.244	0.472	0.575	1.626	-9.207
ASP-3	0.075	-0.244	1	-0.291	-0.356	1.150	0.001
AVP-7	-0.130	0.472	-0.291	1	0.822	3.405	0.103
TDB1v	-0.348	0.575	-0.356	0.822	1	4.899	0.949

Table 5: Various interaction between the top ranking compoundsand the active site of 5T8E androgen receptor

S/No.	Binding affinities	H- Bond Interactions	Hydrophobic and Electrostatic interactions
19	-10.6	GLU683 Conventional H- Bond	ARG752 ASN756 TRP751 TRP751 VAL684 ARG752 ALA748 PRO628
5	-10.5	GLU681 Conventional H- Bond	ARG752 TRP751 LEU805 TRP751 VAL715 ALA748 PRO682
			ARG752
8	-10.4	GLU681 Conventional H- Bond	ARG752 ASN756 TRP751 VAL715 ALA748 LEU805 TRP751 PRO682 ARG752

Table 6: Drug- likeness properties of the top ranking compounds

S/N	MW	HBA	HBD	Synthetic accessibility	Bio availability score	Drug-likeness
19	425.48	4	1	3.71	0.55	YES
5	414.93	2	1	3.45	0.55	YES
8	394.51	2	1	3.60	0.55	YES

Table 7: ADMET properties prediction of the top ranking compounds

Properties	Compound 19	Compound 5	Compound 8
Absorption			
Caco- 2 permeability	-5.13	-5.18	-5.18
Pgp- inhibitor	High probability	High probability	High probability
Pgp- substrate	Low probability	Low probability	Low probability
Human intestinal absorption	1.4%	2.1 %	5.6%
Distribution			
BBB penetration	Low	Low	Low
Metabolism			
CYP1A2 inhibitor	High	High	High
CYP1A2 substrate	Moderate	Moderate	Moderate
CYP2C19 inhibitor	High	Moderate	Moderate
CYP2C19 substrate	Low	Low	Low
CYP2C9 inhibitor	Moderate	Moderate	Moderate
CYP2C9 substrate	High	High	High
CYP2D6 inhibitor	Low	Low	Low
CYP2D6 substrate	High	High	High
CYP3A4 inhibitor	Low	Low	Low
CYP3A4 inhibitor	Low	Low	Low
Excretion			
Clearance (mL/min/Kg)	5.389	4.886	5.839
$T_{1/2}$	Short	Short	Short
Toxicity			
AMES Toxicity	Low probability	Low probability	Low probability
Skin Sensitization	Low probability	Low probability	Low probability

Carcinogenicity	Low probability	Low probability	Low probability
Eye Corrosion	Low probability	Low probability	Low probability
Eye Irritation	High probability	Low probability	Low probability
Respiratory Toxicity	High probability	High probability	High probability

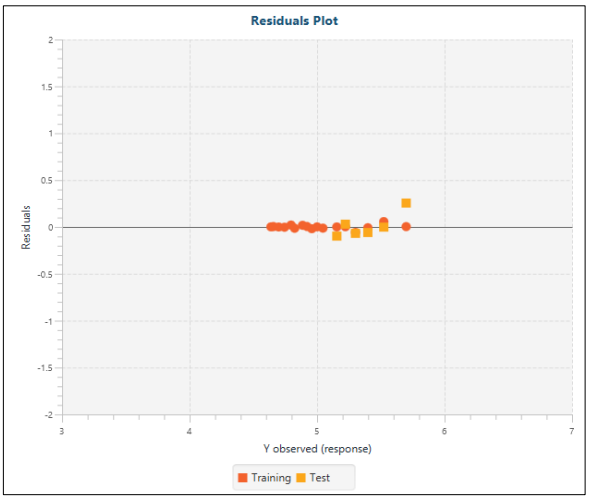

Figure 2: Scatter plot of standardized residual versus the Investigational activities

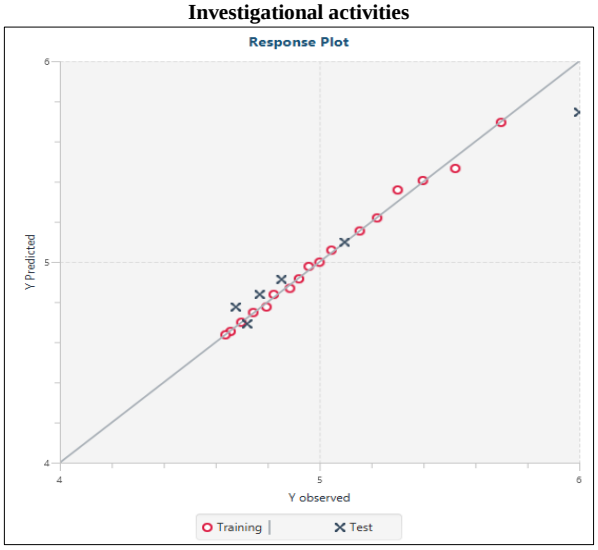

Figure 3: Scatter plot of biological activities against calculated activities

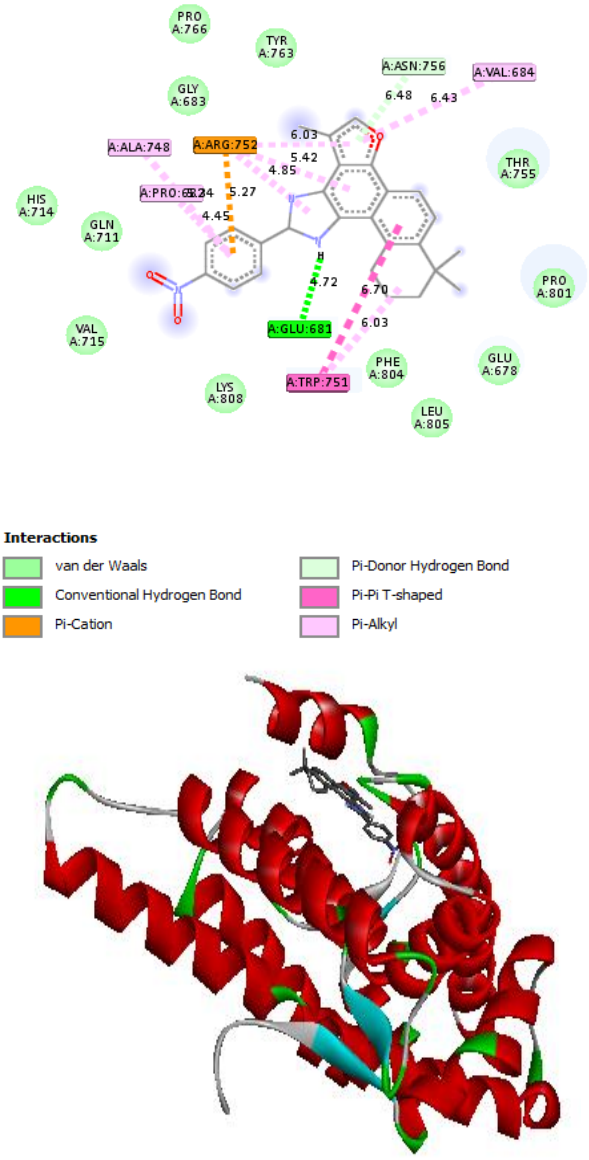

Figure 4: 2Dand 3D pictorial of compound 19 with 5T8E androgen receptor

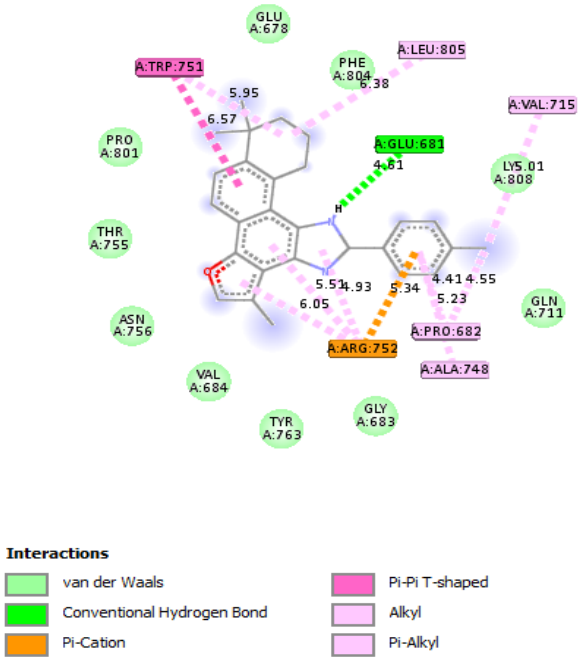

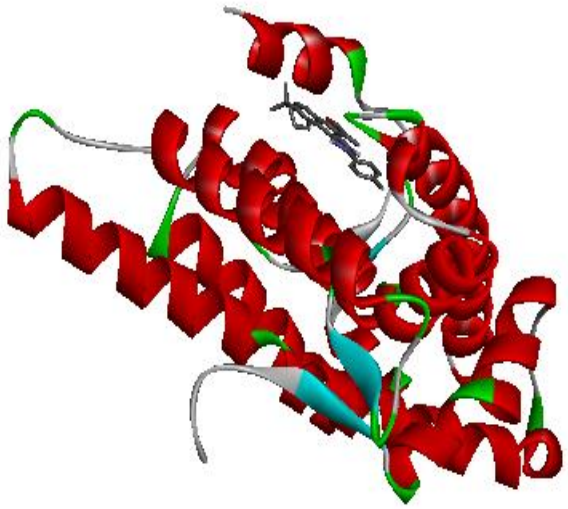

Figure 5: 2Dand 3D pictorial of compound 5 with 5T8E androgen receptor

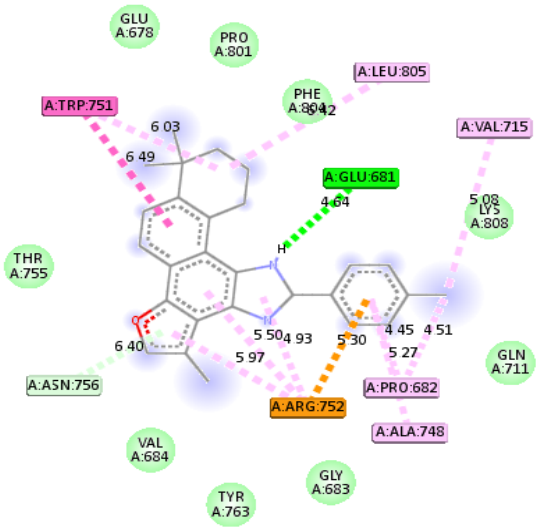

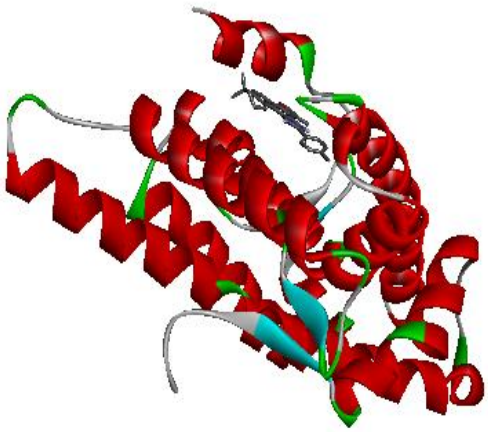

Figure 6: 2Dand 3D pictorial of compound 8 with 5T8E androgen receptor

4. Conclusion and Future Scope

In conclusion, model one was found to be predictive, powerful, and reliable, based on the following statistical parameters: coefficient of determination (R^2) = 0.9916, adjusted R^2 = 0.9878, standard error of estimation (SEE) = 0.346, mean absolute error (MAE) = 0.035, and concordance correlation coefficient (CCC) = 0.9238. Also, the model shows anticancer activity of tanshinone derivatives on the THSA, MLFER_E, ASP-3, AVP-7, and TDB1v descriptors. Based on the molecular docking results, the docking scores of the three most promising compounds were found to be between (-10.4 to -10.6 kcal/mol) respectively. Drug- likeness and ADMET predictions revealed favorable characteristics for the test compounds. These results indicate that the compounds have promising anticancer potential, warranting further exploration. Modifying these molecules by introducing appropriate functional groups to enhance their binding affinity with the target receptor could lead to

improved efficacy and therapeutic performance. Therefore, this study demonstrates that computational approaches can effectively complement experimental research, providing valuable insights and stronger justification in the ongoing search for treatments against various diseases

Acknowledgements- The authors thanked Department of Pure and Applied Chemistry, Adamawa State University, Mubi.

Funding Source- This research did not received any grant from funding agency

Authors' Contributions- AIK design and performed the experiment, wrote the paper. SMA performed experiment and wrote the paper.

Conflict of Interest- Authors declare no conflict of interest

Data Availability- None

References

[1] Solomon, V. R.; Hua, C.; Lee, H., "Hybrid pharmacophore design and synthesis of isatin-benzothiazole analogs for their anti-breast cancer activity," *Bioorg. Med. Chem*., Vol.17, pp 7585-7592. 2009.

[2] Chandrappa S, Kavitha CV, Shahabuddin MS, Vinaya K, Ananda Kumar CS, Rangantha SR., "synthesis of 2-(5-(4-chlorophenyl)furan-2-yl)methylene)-4-oxo-2-thiooxo-thiazolidin-3-yl)acetic acid derivatives and evaluation of their cytotoxicity and induction of apoptosis in human leukemia cells," *Bioorganic & Medicinal Chemistry*, Vol.17, Issue.6, pp.2576- 84. 2009

[3] Al-Suwaidan IA, Abdel-Aziz AA-M, Shawer TZ, Ayyad RR, Alanazi AM, El-Morsy AM, Mohamed MA, Abdel-Aziz NI, El-Sayed MA-A, El-Azab AS., "Synthesis, antitumor activity and molecular docking study of some novel3-benzyl-4 (3H) quinazolinone analogues," *Journal of Enzyme Inhib Med Chem*., Vol.31, Issue.1, pp.78–89. 2016.

[4] Nelen, V., "Epidemiology of Prostate Cancer. In: Ramon, J., Denis, L.J. (eds) Prostate Cancer," *Recent Results in Cancer Research*, Vol.175, Springer, Berlin, Heidelberg, pp.1- 8. 2007.

[5] Rawla P., "Epidemiology of prostate cancer," *World J Oncol.*, Vol.10, pp.63-89. 2019.

[6] Siegel, R., Naishadham, D. and Jemal, A., "Cancer Statistics," *CA: A Cancer Journal for Clinicians*, Vol.63, pp.11 - 30. 2013.

[7] Siegel, R.L., Miller, K.D. and Jemal, A., "Cancer Statistics," *201. CA: A Cancer Journal for Clinicians*, Vol.65, pp.5- 29. 2015.

[8] G. Attard, C. Parker, R. A. Eeles, F. Schr¨oder, S. A Tomlins, I. Tannock, C. G. Drake and J. S. de Bono, "Prostate cancer," *Lancet.* Vol.387, pp.70- 82, 2016.

[9] Horoszewicz JS, Leong SS, Kawinski E, Karr JP, Rosenthal H, Chu TM, Mirand EA, Murphy GP., "LNCaP model of human prostatic carcinoma.," *Cancer Res.,* Vol.43, Issue.4, PMID: 6831420, pp.1809-18. 1983.

[10] van Bokhoven A, Varella-Garcia M, Korch C, Johannes WU, Smith EE, Miller HL, Nordeen SK, Miller GJ, Lucia MS., "Molecular characterization of human prostate carcinoma cell lines," *Prostate*, Vol.57, Issue.3,PMID: 14518029 pp.205-25.2003.

[11] Leelananda, Sumudu P., and Steffen Lindert, "Computational methods in drug discovery," *Beilstein journal of organic chemistry*, Vol.12, Issue.1, pp.2694-2718, 2016.

[12] Hillisch A, Pineda LF, Hilgenfeld R., "Utility of homology models in the drug discovery process," *Drug Discov Today*, Vol.9, Issue.15 PMID: 15279849 pp.659- 69. 2004.

[13] Siegel RL, Miller KD, Jemal A., "Cancer statistics," *CA Cancer J Clin.*, Vol.66, Issue.1, PMID: 26742998 pp.7-30. 2016.

[14] Wojciechowska U, Didkowska J., "Illness and deaths from malignant tumors in Poland," *National Cancer Registry, Cancer Centre - Institute for them. Maria Sklodowska-Curie*, ISSN 0867–8251. 2013.

[15] Li H, Li X, Bai M, Suo Y, Zhang G, Cao X., "Matrine inhibited proliferation and increased apoptosis in human breast cancer MCF-7 cells via up regulation of Bax and down regulation of Bcl-2," *Int J Clin Exp Pathol.*, Vol.8, Issue.11, PMID: 26823806 pp.14793-9. 2015.

[16] Walczak JR, Carducci MA., "Prostate cancer: a practical app. roach to current management of recurrent disease," *Mayo Clin Proc, Vol.*82, pp.243– 249. 2007.

[17] Huang SY, Chang SF, Liao KF, Chiu SC., "Tanshinone IIA Inhibits Epithelial-Mesenchymal Transition in Bladder Cancer Cells via Modulation of STAT3-CCL2 Signaling," *Int J Mol Sci.,* Vol.18, Issue.8, pp.1616. PMID: 28757590, 2017.

[18] Munagala R, Aqil F, Jeyabalan J, Gupta RC., "Tanshinone IIA inhibits viral oncogene expression leading to apoptosis and inhibition of cervical cancer," *Cancer Lett.,* Vol. 356(2 Pt B): PMID: 25304375, pp.536-46. 2015.

[19] Chang TW, Lin CY, Tzeng YJ, Lur HS., "Synergistic combinations of tanshinone IIA and trans-resveratrol toward cisplatin-comparable cytotoxicity in HepG2 human hepatocellular carcinoma cells," *Anticancer Res.,* Vol. 34, Vol.10, PMID: 25275043 pp.5473-80. 2014.

[20] Wang Y, Song D, Costanza F, Ji G, Fan Z, Cai J, Li Q., "Targeted delivery of tanshinone IIA-conjugated mPEG-PLGA-PLL-cRGD nanoparticles to hepatocellular carcinoma," *J Biomed Nanotechnol*, Vol.10, Issue.11, PMID: 26000384**, *pp.***3244-52. 2014.

[21] Li, Chunlong, et al., "The interplay between autophagy and apoptosis induced by tanshinone IIA in prostate cancer cells," *Tumor Biology, Vol.* 37, pp.7667-7674, 2016.

[22] Ketola K, Viitala M, Kohonen P, Fey V, Culig Z, Kallioniemi O, Iljin K., "High-throughput cell-based compound screen identifies pinosylvin methyl ether and tanshinone IIA as inhibitors of castration-resistant prostate cancer," *J Mol Biochem.,* Vol.5, Issue.1, PMID: 27891324, pp.12-22. 2016.

[23] Liu W, Zhou J, Geng G, Shi Q, Sauriol F, Wu JH., "Antiandrogenic, maspin induction, and antiprostate cancer activities of tanshinone IIA and its novel derivatives with modification in ring A., "*J Med Chem..*, Vol.55, Issue.2, PMID: 22175694, pp.971-975. 2012.

[24] Xu D, Lin TH, Zhang C, Tsai YC, Li S, Zhang J, Yin M, Yeh S, Chang C. The selective inhibitory effect of a synthetic tanshinone derivative on prostate cancer cells," *Prostate.*, Vol.72, Issue.7, PMID: 21932429, pp.803-16, 2012.

[25] Wang H, Su X, Fang J, Xin X, Zhao X, Gaur U, Wen Q, Xu J, Little PJ, Zheng W., "Tanshinone IIA Attenuates Insulin Like Growth Factor 1 -Induced Cell Proliferation in PC12 Cells through the PI3K/Akt and MEK/ERK Pathways," *Int J Mol Sci.,* Vol.19, Issue.9, pp.2719 PMID: 30213025. 2018.

[26] Wang M, Zeng X, Li S, Sun Z, Yu J, Chen C, Shen X, Pan W, Luo H., "A Novel Tanshinone Analog Exerts Anti-Cancer Effects in Prostate Cancer by Inducing Cell Apoptosis, Arresting Cell Cycle at G2 Phase and Blocking Metastatic Ability," *Int J Mol Sci.,* Vol.20, Issue.18, pp.4459, PMID: 31510010. 2019.

[27] Xu D, Hu H, Guan J, Da J, Xie Y, Liu Y, Kong R, Song G, Zhou H., "Synthesis of novel tanshinone derivatives for treatment of castration-resistant prostate cancer," *Chem Biol Drug Des.,* Vol.94, Issue.3, PMID: 31108007, pp.1656-1663. 2019.

[28] Yunusa U, Umar U, Idris S, Kubo A, Abdullahi T., "Experimental and DFT computational Insights on the adsorption of selected pharmaceutical of emerging concern from water system Onto magnetically modified biochar," *Journal of the Turkish Chemical Society, Section A Chemistry*, Vol.8, Issue.4, pp.1179- 1196. 2021

[29] Yunusa, Umar, et al., "Theoretical Investigations and Experimental Studies of the Adsorption of Diethyl Phthalate and Di (2-ethylhexyl) Phthalate on Reduced Graphene Oxide," *Applied Journal of Environmental Engineering Science, Vol.* 7, Issue.2, pp.151- 168. 2021.

[30] Tropsha A, Bajorath Jr., "Computational methods for drug discovery and design, ACS Publications," *Journal of Medicinal Chemistry*, Vol.59, Issue.1, 2015.

[31] Beheshti A, Pourbasheer E, Nekoei M, Vahdani S., "QSAR modeling of antimalarial activity of urea derivatives using genetic algorithm- multiple linear regressions," *Journal of Saudi Chemical society*, Vol.20, Issue.3, pp.282- 290. 2016.
[32] Minovski N, Župerl Š, Drgan V, Novič M., "Assessment of app.licability domain for multivariate counter-propagation artificial neural network predictive models by minimum euclidean distance space analysis: a case study," *Anal Chim Acta*., Vol.759. PMID: 23260674, pp.28-42. 2013.
[33] Chirico N, Gramatica P., "Real external predictivity of QSAR models: how to evaluate it? Comparison of different validation criteria and proposal of using the concordance correlation coefficient," *J Chem Inf Model*. Vol.51, Issue.9, PMID: 21800825, pp.2320-35. 2011.
[34] Connolly, Michael L., "Analytical molecular surface calculation," *Applied Crystallography*, Vol.16, Issue.5, pp.548-558. 1983.
[35] Rojas, H., Ritter, C., & Pizzol, F. D., "Mechanisms of dysfunction of the blood-brain barrier in critically ill patients: emphasis on the role of matrix metalloproteinases," *Revista Brasileira De Terapia Intensiva*, Vol.23, pp.222-227. 2011.
[36] Wang, J., & Hou, T., "Recent advances on in silico ADME modelling," *Annual reports in computational chemistry*, Vol.5, pp.101-127. 2009.
[37] Ma XL, Chen C, Yang J., "Predictive model of blood-brain barrier penetration of organic compounds," *Acta Pharmacol Sin.*, Vol.26, Issue.4, PMID: 15780201, pp.500-12. 2005.
[38] Yamashita S, Furubayashi T, Kataoka M, Sakane T, Sezaki H, Tokuda H., "Optimized conditions for prediction of intestinal drug permeability using Caco-2 cells," *Eur J Pharm Sci.*, Vol.10, Issue.3, PMID: 10767597, pp.195-204. 2000.
[39] Horie, Kazutoshi, Fuxing Tang, and Ronald T. Borchardt, "Isolation and characterization of Caco-2 subclones expressing high levels of multidrug resistance protein efflux transporter," *Pharmaceutical research*, Vol.20, pp.161-168, 2003.
Chen W, Tang F, Horie K, Borchardt RT, "CACO-2 cell monolayers as a model for studies of drug transport across human intestinal epithelium," *In: Lehr KM (ed) Cell culture models of biological barriers, Taylor and Francis*, New York, pp 143–163, 2002.

AUTHORS PROFILE

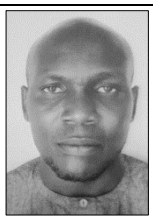

Abdulrahman Ibrahim Kubo B.Sc, M.Sc. in Physical/ Computational Chemistry from University of Maiduguri and Yobe State University Damaturu in 2011 and 2025.
Current Position: Assistant Lecturer in the Department of Pure and Applied Chemistry Adamawa State University, Mubi. He is a member of Chemical Society of Nigeria and Institute of Chartered Chemist of Nigeria.
Research Interest: Cancer drug design

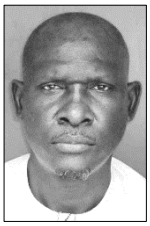

Saminu M. A M.Tech. in Industrial Chemistry from Modibbo Adama University, Yola, Nigeria.
Current Position: Assistant Chief Technologist in the Department of Pure and Applied Chemistry, Adamawa State University, Mubi.

